Importance of the sea surface curvature to interpret the normalized radar cross section

A. A. Mouche,[1,2] B. Chapron,[1] N. Reul,[1] D. Hauser,[3] and Y. Quilfen[1]

[1] Asymptotic models (small perturbation and small slope approximation at first-order, Kirchhoff approximation or two-scale model) used to predict the normalized radar cross section of the sea surface generally fail to reproduce in detail backscatter radar measurements. In particular, the predicted polarization ratio versus incidence and azimuth angles is not in agreement with experimental data. This denotes the inability of these standard models to fully take into account the roughness properties with respect to the sensor's configuration of measurement (frequency, incidence, and polarization). On the basis of particular assumptions, to decompose the scattered electromagnetic field between zones covered with freely propagating waves and others where roughness and slopes are enhanced, recent works were able to match observations. In this paper, we do not assume such a decomposition but study the latest improvements obtained in the field of approximate scattering theories of random rough surfaces using the local and resonant curvature approximations. These models are based on an extension of the Kirchhoff Approximation up to first order to relate explicitly the curvature properties of the sea surface to the polarization strength of the scattered electromagnetic field. Consistency with previous approaches is discussed. As shown, dynamically taking into account the sea surface curvature properties of the surface is crucial to better interpret normalized radar cross-section and polarization ratio sensitivities to both sensor characteristics and geophysical environment conditions. The proposed developments, termed the Resonant Curvature Approximation (RCA), are found to reproduce experimental data versus incidence angle and azimuth direction. The polarization sensitivity to the wind direction and incidence angle is largely improved. Finally, Gaussian statistical assumption adopted to derive the analytical expression of the normalized radar cross section is also discussed. In particular, the third-order cumulant function is shown to better reproduce the second-order up-/down-wind azimuth modulation. The proposed developments appear very promising for improvement of our understanding and analysis of both sea surface radar backscatter and Doppler signals.

1. Introduction

[2] As the capabilities of remote sensing instruments ever increase, opportunities to develop consistent inversion schemes of the sea surface geometry and kinematic appear. For instance, the high-resolution SAR images are now commonly used to retrieve wind fields thanks to the backscattered intensity power [*Monaldo and Kerbaol*, 2003] or the sea surface velocity using the Doppler anomaly analysis [*Chapron et al.*, 2004, 2005]. Consistent inversion schemes merging these two sources of information are promising. In particular, this will help to better decipher between wind effects and current impacts on the apparent surface roughness [*Quilfen et al.*, 2001; *Kelly et al.*, 2001; *Park et al.*, 2006].

[3] However, to date, large discrepancies between observations and model predictions still remain to preclude consistent inversions. Numerous efforts to consider theoretically based asymptotic solutions [e.g., *Plant*, 2002] still fail to correctly reproduce the normalized radar cross section (NRCS) in both HH and VV copolarizations under all environmental conditions, sensor configurations and characteristics. *Mouche et al.* [2005] show that the C band polarization ratio (PR), defined as the ratio of the VV NRCS over HH NRCS, is azimuth dependent with respect to the wind direction for incidences larger than $30°$. *Mouche et al.* [2006] show that a first-order expansion for asymptotic electromagnetic solutions will fail to reproduce this azimuth dependency. By construction, small slopes or elevations expansions cannot reproduce any azimuthal variation for the

[1]Laboratoire d'Océanographie Spatiale, Ifremer, Plouzané, France.
[2]Also at Centre National d'Etudes Spatiales, Paris, France.
[3]Centre d'Etude des Environnements Terrestre et Planétaires, IPSL, CNRS/UVSQ, Vélizy, France.
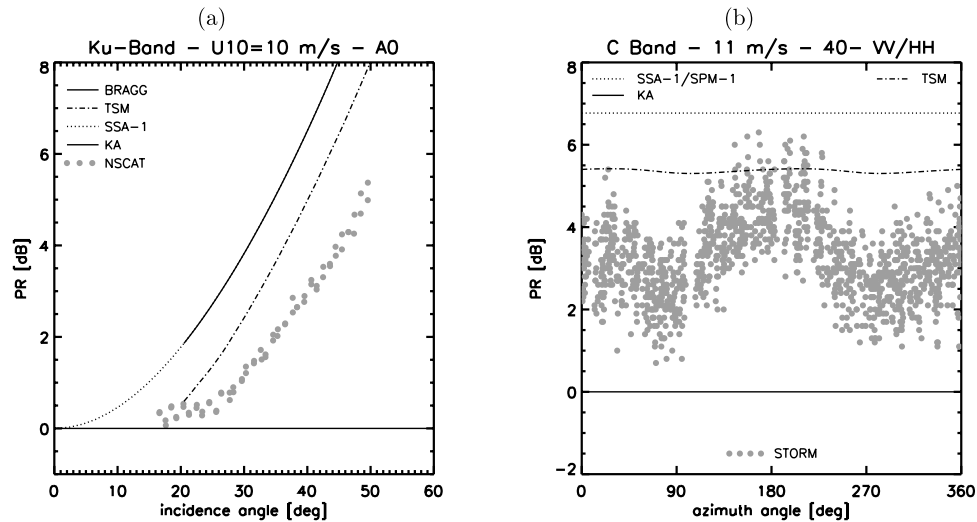
Figure 1. (a) Polarization ratio versus incidence angle in Ku band for a 10 m/s in the case of an isotropic sea surface. (b) Polarization ratio versus wind direction relative to the radar's azimuth look direction for a 11 m/s wind speed and a 40° incidence angle.

PR. A two-scale model (TSM) [*Valenzuela*, 1978; *Plant*, 1986] would lead to an azimuth dependency, but generally not in agreement with the data. In the TSM formalism, the large tilting waves are the source of depolarization effects on the Bragg resonant waves. Recent works [*Kudryavtsev et al.*, 2003, 2005; *Mouche et al.*, 2006; *Voronovich and Zavarotny*, 2001] are based on particular statistical decomposition for the NRCS. In such developments, the sea surface is assumed to follow a double structure. The scattered electromagnetic field is separated in two contributions: $\vec{E} = \vec{E}_S + \vec{E}_B$. $\vec{E}_S$ corresponds to solutions over the regular part of the surface and $\vec{E}_B$ to solution over the nonregular part of the surface. The resulting cross section is found under the assumption that $\vec{E}_S$ and $\vec{E}_B$ are separated in space and independent. Thus the total cross section is the sum of two contributions, i.e., regular surface and enhanced roughness areas. For the regular part of the surface, a two-scale model (or SSA-2) approach is valid as both tilting and tilted waves (or small slopes) are not extreme. For the nonregular surface, such as breaking areas with larger slopes, a GO solution is used, and this NRCS part is then proportional to the breaking surface probability density function. This is the strength of such methods (because it can help to interpret the measurements in terms of sea surface process). However, one underlying problem lies in the definition of each sea surface process used as input of each separated electromagnetic model invoked. More specifically, a crucial question is to define their respective spectral forms or the range of wavenumbers of the wave spectrum to consider for their descriptions.

[4] To go beyond the TSM's formalism with the arbitrary choice to separate large modulating and small modulated waves, *Elfouhaily et al.* [2003a] proposed an asymptotic theory based on Kirchhoff Approximation (KA) taking into account the curvature effect of the surface on the polarization state of the scattered field. On the basis of both analytical comparisons with TSM and data comparisons, the proposed solution, termed LCA-1, exhibits polarization sensitivity very close to TSM [*Mouche et al.*, 2007a]. This

model is thus somehow inadequate to reproduce the NRCS of the ocean surface. However, contrary to the TSM, LCA-1 solution is more general and dynamically unifies small perturbation (SPM) and high-frequency (KA) asymptotic solutions. It further removes the issue concerning the dividing tilting scale. A solution which provides a more realistic polarization sensitivity than LCA-1, without invoking any arbitrary separation of the ocean surface scales, has then been proposed to restrict the curvature correction to the resonant Bragg waves [*Mouche et al.*, 2007a]. This model, namely the Resonant Curvature Approximation (RCA), conserves the dynamical properties of LCA-1. Accordingly, the polarization ratio at a given incidence angle will be sea surface roughness dependent, i.e., wind speed and direction dependent.

[5] In this paper, data and model comparisons are used to illustrate these developments. We briefly present the asymptotic solutions to take into account the surface curvature effect. Issues about the statistical representation of the sea surface are also commented to approach the up-/down-wind asymmetry of the observed NRCS. Conclusions and perspectives for the use of these models in the field of ocean remote sensing ends this work.

2. Position of the Problem

[6] To date, there is no asymptotic electromagnetic model able to reproduce the NRCS in both VV and HH polarizations for all incidence angles, radar wavelength and wind conditions (speed, direction), without invoking a particular separation of the ocean surface between two different structures [e.g., *Phillips*, 1988]. Figure 1 illustrates this point with two examples of PR in Ku and C band. This quantity allows comparisons between model and data without calibration issues and is thus adequate to evaluate and discuss the polarization sensitivity of electromagnetic models. In Figure 1a, we present the PR versus incidence angle calculated from Ku band NRCS in both VV and HH polarizations measured by NSCAT. The data acquired in Ku band were already presented by *Quilfen et al.* [1999]. We

consider incidence angles from 20° to 50° for a 10 m/s wind speed. Here a_0^{pp} stands for the zeroth-order coefficient of the standard three-term Fourier model used for empirical formulations of the NRCS versus viewing angle with respect to wind direction,

$$\sigma_0^{pp}(U, \theta, \Phi) = a_0^{pp}(U, \theta) + a_1^{pp}(U, \theta)\cos(\Phi) + a_2^{pp}(U, \theta)\cos(2\Phi), \tag{1}$$

where U is the near-surface wind speed, θ the radar's incidence angle and Φ the wind direction relative to the radar's azimuth look direction. Here pp denotes the copolarization considered. Model predictions are also presented. The sea surface description used in these models is given by the unified spectrum for short and long wind-driven waves proposed by *Elfouhaily et al.* [1997]. To be consistent with these observations, we only consider the isotropic part of the spectrum. Analytical NRCS expressions of the different models are recalled in the appendix. As already reported [e.g., *Kudryavtsev et al.*, 2003], SPM-1 underestimates the NRCS in HH polarization whereas it is rather good for the VV polarization. The direct consequence is an overestimation of the PR. Adding a modulation from the longer waves to the resonant Bragg waves through a TSM improves the predicted NRCS. However, NRCS in HH polarization is lower than the measurements and TSM's PR is not in agreement with the data. The Small Slope Approximation model (SSA-1) [*Voronovich*, 1994], by construction, imposes a strong polarization sensitivity and is inadequate. This comes from the fact that as the incidence angle increases, SSA-1 tends very quickly to the SPM-1 asymptotic solution. To lower this effect, higher orders of SSA must be considered. However, *Voronovich and Zavarotny* [2001] showed that addition of the second order is not sufficient. To match observations, solutions reported by *Kudryavtsev et al.* [2003] or *Voronovich and Zavarotny* [2001] are then built on an apparent necessary division of the ocean scene in zones with smooth surface waves and others with enhanced roughness and slopes elements, primarily associated to breaking waves.

[7] In Figure 1b, we present the PR versus azimuth angle obtained from the NRCS in both VV and HH polarizations measured by the STORM radar. A complete presentation of this radar and the data set is given by *Hauser et al.* [2003] and *Mouche et al.* [2006]. For illustration purpose, we consider a 40° incidence angle and a 11 m/s wind speed. As clearly illustrated, a measurable azimuthal PR modulation is observed.

3. Extended Kirchhoff Model for the Normalized Radar Cross Section

[8] Hereafter, we briefly recall notations and developments.

3.1. Coordinates System and Definitions

[9] The right cartesian coordinate system is defined by the triplet of normalized vectors $(\hat{x}, \hat{z})$, where the z axis is directed upward. The sea surface elevation is represented by $z = \eta(x, y) = \eta(\boldsymbol{r})$, where $\boldsymbol{r}$ is the horizontal component of the three-dimensional position wave vector $\boldsymbol{R} = (\boldsymbol{r}, z)$. We consider an incident downward propagating electromagnetic plane wave with a wave-vector $\boldsymbol{K}_0 = (\boldsymbol{k}_0, -q_0)$. The up-

going scattered waves are characterized by the wave-vector $\boldsymbol{K} = (\boldsymbol{k}, q_k)$. $\boldsymbol{k}_0$ and $\boldsymbol{k}$ are the horizontal components of the incident and scattered waves whereas q_0 and q_k are the vertical ones. We define also $\boldsymbol{Q}_H$ and Q_z related to the coordinates of the wave numbers $\boldsymbol{K}$ and $\boldsymbol{K}_0$: $\boldsymbol{Q}_H = \boldsymbol{k} - \boldsymbol{k}_0$ and $Q_z = q_0 + q_k$.

[10] The scattered field above and far away $(R \rightarrow \infty)$ from the sea surface is assumed to be related to the incident wave through the relation

$$\boldsymbol{E}_s(\boldsymbol{R}) = -2i\pi \frac{e^{iKR}}{R} \mathbb{S}(\boldsymbol{k}, \boldsymbol{k}_0) \cdot \hat{E}_0. \tag{2}$$

$\mathbb{S}(\boldsymbol{k}, \boldsymbol{k}_0)$ is the so-called scattering operator. $\boldsymbol{E}_s(\boldsymbol{R})$ and $\mathbb{S}(\boldsymbol{k}, \boldsymbol{k}_0)$ can be decomposed on the fundamental polarization basis:

$$\boldsymbol{p}_v^\pm(\pm k) = \frac{k\hat{z} \mp q_k\hat{k}}{K} \qquad \boldsymbol{p}_h^\pm(\pm k) = \hat{z} \times \hat{k}, \tag{3}$$

where the subscripts v and h indicate the vertical and horizontal polarizations, respectively. The minus superscript corresponds to the down-going plane waves while the plus superscript to the up-going waves. In this vectors basis, the scattering operator is related to the scattering amplitude 2×2 matrix through

$$\mathbb{S}(\boldsymbol{k}, \boldsymbol{k}_0) = \begin{bmatrix} \boldsymbol{p}_v^-(\boldsymbol{k}_0) \\ \boldsymbol{p}_h^-(\boldsymbol{k}_0) \end{bmatrix}^T \cdot \begin{bmatrix} \mathbb{S}^{vv}(\boldsymbol{k}, \boldsymbol{k}_0) & \mathbb{S}^{vh}(\boldsymbol{k}, \boldsymbol{k}_0) \\ \mathbb{S}^{hv}(\boldsymbol{k}, \boldsymbol{k}_0) & \mathbb{S}^{hh}(\boldsymbol{k}, \boldsymbol{k}_0) \end{bmatrix} \cdot \begin{bmatrix} \boldsymbol{p}_v^+(\boldsymbol{k}) \\ \boldsymbol{p}_h^+(\boldsymbol{k}) \end{bmatrix}, \tag{4}$$

where the superscript T stands for the transpose operator. In the 2×2 matrix, the first subscript indicates the incident polarization whereas the second one indicates the scattered polarization configuration considered.

[11] For a given polarization configuration pq, $\mathbb{S}^{pq}(\boldsymbol{k}, \boldsymbol{k}_0)$ is further written as

$$\mathbb{S}^{pq}(\boldsymbol{k}, \boldsymbol{k}_0) = \frac{1}{Q_z} \int_{\boldsymbol{r}} \mathbb{N}^{pq}(\boldsymbol{k}, \boldsymbol{k}_0; \eta(\boldsymbol{r})) e^{-iQ_z\eta(r)} e^{-i\boldsymbol{Q}_H \cdot \boldsymbol{r}} d\boldsymbol{r}, \tag{5}$$

where $\mathbb{N}^{pq}(\boldsymbol{k}, \boldsymbol{k}_0; \eta(\boldsymbol{r}))$ is a kernel depending on the approach considered to establish the solution.

[12] The scattering cross section is given by the incoherent second-order statistical expression

$$\sigma^{pq} = \langle |\mathbb{S}^{pq}(\boldsymbol{k}, \boldsymbol{k}_0)|^2 \rangle - |\langle \mathbb{S}^{pq}(\boldsymbol{k}, \boldsymbol{k}_0) \rangle|^2. \tag{6}$$

3.2. Local and Resonant Curvature Approximations

[13] On the basis of *Elfouhaily et al.* [2003b, 2003a] developments, the scattering matrix expansion up to the first order is

$$\begin{aligned} \mathbb{S}^{pq}(\boldsymbol{k}, \boldsymbol{k}_0) = {} & \frac{\mathbb{K}(\boldsymbol{k}, \boldsymbol{k}_0)}{Q_z} \int_{\boldsymbol{r}} e^{-iQ_z\eta(r)} e^{-i\boldsymbol{Q}_H \cdot \boldsymbol{r}} d\boldsymbol{r} \\ & - i \int_{\boldsymbol{r}} \int_{\boldsymbol{\xi}} T(\boldsymbol{k}, \boldsymbol{k}_0; \boldsymbol{\xi}) \hat{\eta}(\boldsymbol{\xi}) e^{-iQ_z\eta(r)} e^{-i(\boldsymbol{Q}_H - \boldsymbol{\xi}) \cdot \boldsymbol{r}} d\boldsymbol{\xi} d\boldsymbol{r}, \end{aligned} \tag{7}$$

where T is written as:

$$T_{\text{lca}}(\boldsymbol{k}, \boldsymbol{k}_0; \boldsymbol{\xi}) = [\mathbb{B}(\boldsymbol{k}, \boldsymbol{k}_0; \boldsymbol{\xi}) - \mathbb{K}(\boldsymbol{k}, \boldsymbol{k}_0)]. \tag{8}$$

$\mathbb{B}$ is the Bragg kernel and $\mathbb{K}$ is the Kirchhoff kernel (see, e.g., *Elfouhaily et al.* [2003a] for their analytical expression). In equation (7), the second term represents a first-order correction to Kirchhoff solution given by the first term to take into account the surface curvature effects on the polarization state of the scattered field. *Mouche et al.* [2007a, Appendix A] showed that, under Gaussian statistics, the NRCS can be written as the sum of two terms: the KA and the first-order contributions. In KA theory, for random surfaces, all the roughness scales are considered through the definition of the statistical characteristic function. For Gaussian random surfaces, this KA solution reduces to the Fourier coefficient of a function solely depending upon the correlation function. This solution already enables to take into account the curvature effect on the backscattering. The effect is particularly noticeable for incidence angles larger than 15°. This curvature effect explains the difference between the GO-like and the Physical Optics (PO) approximations. For LCA, the kernel $T(\boldsymbol{k}, \boldsymbol{k}_0, \boldsymbol{\xi}) \propto \boldsymbol{\xi}^2$ is quadratic and fully reflects the potential surface curvature effect on the polarized sensitivity. This first-order expansion has the property to reach dynamically both KA and SPM-1 limits with respect to the frequency and the properties of the surface considered. Here $\hat{\eta}(\boldsymbol{\xi})$ is the Fourier transform of the surface height function $\eta(\boldsymbol{r})$, $\boldsymbol{\xi}$ the wave number of the surface in the spectral domain.

[14] In work by *Mouche et al.* [2007a], we consider a formulation which conserves all the dynamic properties of this proposed solution but with a weaker polarization sensitivity. In particular, as proposed by *Shaw and Dougan* [1998] from a Green's function refinement, the curvature effect is solely limited to the resonant Bragg waves. In this case, the kernel expression T is simply

$$T_{\mathrm{rca}}(\boldsymbol{k}, \boldsymbol{k}_0; \boldsymbol{\xi}) = [\mathbb{B}(\boldsymbol{k}, \boldsymbol{k}_0; \boldsymbol{\xi}) - \mathbb{K}(\boldsymbol{k}, \boldsymbol{k}_0)]\delta(\boldsymbol{\xi} - \boldsymbol{Q}_H). \quad (9)$$

[15] Assuming Gaussian statistics for the sea surface description, the derivation of the NRCS for any expansion such as $\mathbb{N}^{pq}(\boldsymbol{k}_0, \boldsymbol{k}) = \mathbb{N}_0^{pq}(\boldsymbol{k}_0, \boldsymbol{k}) + \int_{\boldsymbol{\xi}} \mathbb{N}_1^{pq}(\boldsymbol{k}_0, \boldsymbol{k}; \boldsymbol{\xi})\, \hat{\eta}(\boldsymbol{\xi})e^{i\boldsymbol{\xi}\cdot\boldsymbol{r}}\, d\boldsymbol{\xi}$ has been performed and discussed in the context of LCA/RCA models [*Mouche et al.*, 2007a]. For LCA, the kernel $N_1(\boldsymbol{k}, \boldsymbol{k}_0, \boldsymbol{\xi}) \propto \boldsymbol{\xi}^2$ is quadratic. In this case, the authors showed that the first-order correction term was nonzero when $\partial^4 \rho(r)/\partial r^4|_{r\,=\,0} \neq 0$, where $\rho(r)$ is the correlation function of the sea surface elevation. Thus, according to LCA, the departure between KA and GO solutions as well as the degree of polarization sensitivity, are both controlled by the mean squared curvature of the random rough surface. Moreover, they showed that this first-order correction is small and can be introduced through a phase perturbation method firstly proposed by *Berman and Dacol* [1990] and further applied by *Voronovich and Zavarotny* [2001]. Thus, in this paper, we consider the first-order term of the scattering matrix expansion to be a small perturbation in the phase term of the zeroth-order contribution in equation (7), such as

$$\mathbb{S}(\boldsymbol{k}, \boldsymbol{k}_0) = \mathbb{K}_0(\boldsymbol{k}, \boldsymbol{k}_0) \int_{\boldsymbol{r}} e^{-iQ_z\eta(\boldsymbol{r})} e^{-iQ_z\delta_{k,k_0\eta(r)}} e^{-i\boldsymbol{Q}_H\cdot\boldsymbol{r}} d\boldsymbol{r}, \quad (10)$$

with

$$\delta_{\boldsymbol{k},\boldsymbol{k}_0}\eta(\boldsymbol{r}) = \int_{\boldsymbol{\xi}} \frac{T_{\mathrm{lca/rca}}(\boldsymbol{k}, \boldsymbol{k}_0; \boldsymbol{\xi})}{\mathbb{K}(\boldsymbol{k}, \boldsymbol{k}_0)} \hat{\eta}(\boldsymbol{\xi})e^{i\boldsymbol{\xi}\cdot\boldsymbol{r}}d\boldsymbol{\xi}. \quad (11)$$

$\tilde{\eta}(\boldsymbol{r}) = \eta(\boldsymbol{r}) + \delta_{\boldsymbol{k},k0}\eta(\boldsymbol{r})$ now becomes a modified surface elevation.

[16] Using this modified surface elevation for the statistical derivation of the NRCS, the characteristic function $\langle e^\eta \rangle$ is replaced by $\langle e^{\tilde{\eta}} \rangle$. Under Gaussian statistics, this formalism enables to have a tractable expression for the NRCS,

$$\sigma_0^{pq}(\theta, \phi) = \left| \frac{\mathbb{K}(\boldsymbol{k}, \boldsymbol{k}_0)}{Q_z} \right|^2 e^{-Q_z^2\tilde{\rho}(0)} \int_{\boldsymbol{r}} \left[e^{Q_z^2\tilde{\rho}(r)} - 1 \right] e^{-i\boldsymbol{Q}_H\cdot\boldsymbol{r}} d\boldsymbol{r}, \quad (12)$$

with:

$$\tilde{\rho}(\boldsymbol{r}) = \int_{\boldsymbol{\xi}} \left| 1 + \frac{T_{\mathrm{lca/rca}}(\boldsymbol{k}, \boldsymbol{k}_0, \boldsymbol{\xi})}{\mathbb{K}(\boldsymbol{k}, \boldsymbol{k}_0)} \right|^2 S(\boldsymbol{\xi})e^{i\boldsymbol{\xi}\cdot\boldsymbol{r}}d\boldsymbol{\xi}. \quad (13)$$

$\tilde{\rho}(\boldsymbol{r})$ is the so-called modified correlation function of a filtered spectrum $S(\boldsymbol{\xi})$, the sea surface elevation spectrum. In the following, we use this formulation.

4. Results and Discussion
4.1. With Gaussian Statistics for the Sea Surface Description

[17] As a first comparison between data and model, we present the PR versus incidence angle given by RCA, LCA-1 and KA for a 10 m/s wind speed in C and Ku band in the case of an isotropic sea surface in Figures 2a and 2b. Since the curvature correction term in RCA is restricted to the resonant Bragg waves, the induced polarization sensitivity is lower than for LCA-1. Indeed, as understood in the framework of extended Kirchhoff theories, in the backscatter case, the polarization sensitivity lies in the definition of the first-order terms in the kernel expansion. The polarization sensitivity measures the relative weight between polarized correction contribution and the nonpolarized contribution of the zeroth-order (KA) term in the scattering matrix expansion. With LCA-1 or RCA extended Kirchhoff solutions, the polarization sensitivity depends on the smallest surface scales. By construction, for LCA-1, the whole contribution of the high-frequency part ($\boldsymbol{\xi} > \boldsymbol{k}_c$) of the spectrum is considered. $\boldsymbol{k}_c$ stands for the implicit cutoff in the wavenumber range of the wave spectrum as $\int_{\boldsymbol{\xi}=\,0}^{\boldsymbol{k}_c} T_{\mathrm{lca}}(\boldsymbol{k}_0, \boldsymbol{k}; \boldsymbol{\xi}) \to 0$. This underlying separating scale in LCA-1 theory was already discussed by *Mouche et al.* [2007a] and explains the similarity of the results between LCA-1 and TSM (see Figures 1a and 2a). With RCA, the small-scale effect on the polarization sensitivity is reduced to the resonant Bragg wave as prescribed by SPM-1 theory or Shaw and Dougan's work [*Shaw and Dougan*, 1998]. The net consequence is that the relative weight of the small-scale effect is dramatically reduced with RCA in comparison with LCA-1. This leads to relatively different polarized contributions, larger for LCA-1, associated to the zeroth-order (KA) term. Compared to Ku and C band data presented here, we have a better agreement with RCA than
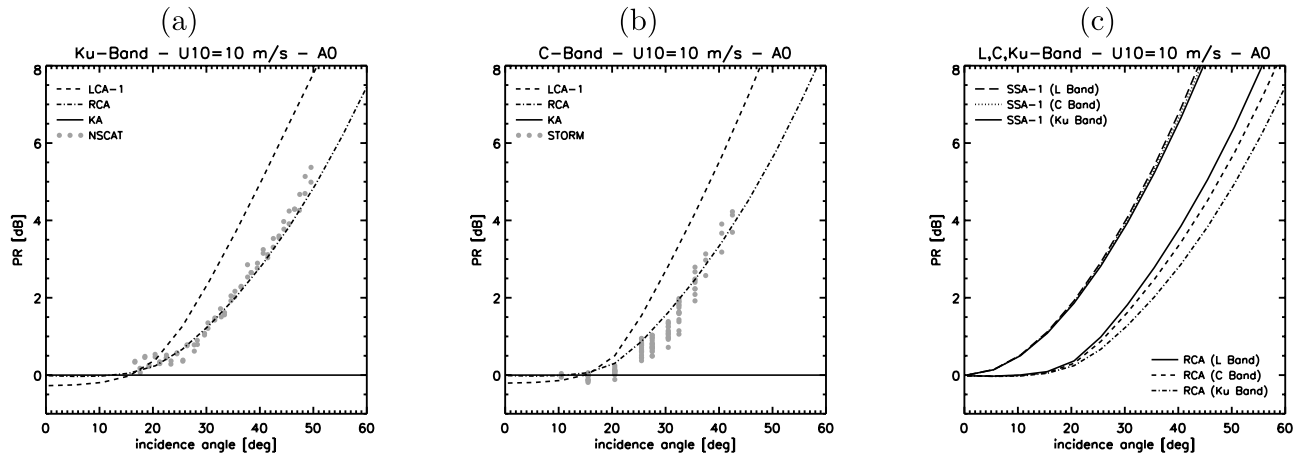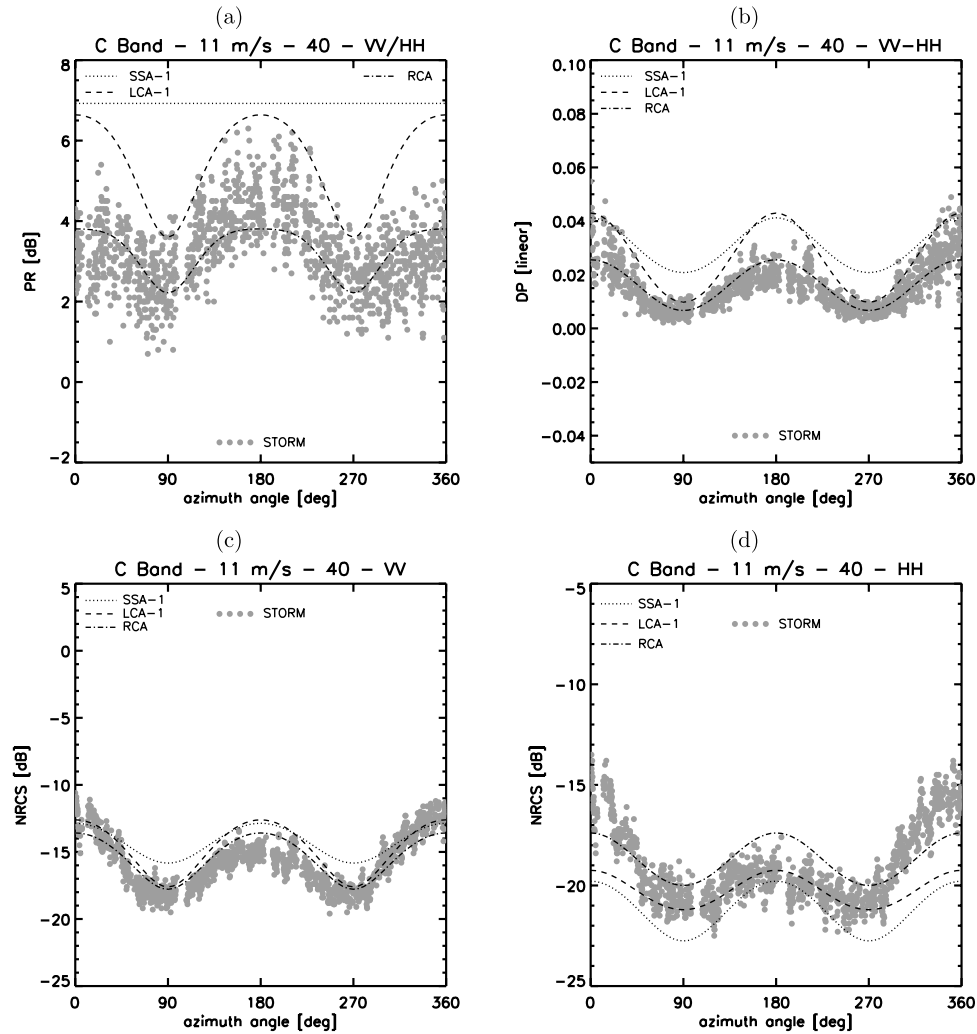
Figure 2. (a) Polarization ratio versus incidence angle in Ku band for a 10 m/s in the case of an isotropic sea surface. Solid, dashed and dash-dotted lines are, respectively, the predictions given by KA, LCA, and RCA models. Data are from NSCAT. (b) Same as Figure 2a but for C band. Data are from STORM radar. (c) Polarization ratio versus incidence angle for a 10 m/s in the case of an isotropic sea surface in Ku, C, and L band given by RCA and SSA-1.

with LCA-1. Interestingly, it can be noticed that the results given by RCA can be compared to the performances achieved by other approaches [*Voronovich and Zavarotny*, 2001; *Kudryavtsev et al.*, 2003; *Mouche et al.*, 2006] based on the spatial decomposition of the sea surface between independently coexisting zones with smooth, small slopes surface waves and others with enhanced roughness and slopes due to breaking waves. As derived, the proposed approach does not explicitly take into account breaking effects. We consider the related information to lie in the sea surface height spectrum definition which, as an overall roughness spectrum, must indeed include the breaking wave signatures. As a consequence, enhanced roughness effects are included in the Kirchhoff integral evaluation (through the correlation function under the Gaussian hypothesis for the surface elevation) and participate to the polarization ratio level. Figure 2c presents the PR predicted by RCA and SSA-1 versus incidence angle for three frequencies. Focusing on the frequency dependency, we observe that the PR decreases when the frequency increases with both models. For SSA-1 (same comments can be done with KA or SPM-1) the frequency dependency is too small. In LCA-1 or RCA, the surface description controls the PR and leads to KA results when $k_0 \rightarrow \infty$ or when the perception of the surface by the sensor is flat (no curvature). Numerical computations of the PR show that the RCA solution is more frequency sensitive than SPM-1, SSA-1 or KA. This explains why the model agrees well with the data in both Ku and C bands in Figures 2a and 2b.

[18] Another important feature in backscattered signals for a given polarization, is the azimuth modulation with respect to the wind direction relative to the radar's azimuth look direction. This modulation helps to infer the wind direction. Data analysis show that this modulation is incidence angle, frequency and polarization dependent. Most electromagnetic models are able to reproduce the first two dependencies. While quite well reproduced in each copolarization, the predicted modulations are not sufficiently polarization sensitive. The comparison in Figure 1 shows

it. In Figures 3a and 4a, we present PR measured with STORM data for two cases (11 and 14 m/s). To show the impact of the curvature model family, we present the results given by LCA-1 and RCA. We also report the SSA-1 results. LCA-1/RCA formalism enables to reproduce an azimuth modulation for the PR due to the curvature correction term. Following the Gaussian statistics for the sea surface representation, the models can only reproduce the second harmonic of the PR. We will see in the next section that this issue can be improved considering skewness effect. Comparisons between LCA-1 and RCA confirm that the mean level of the PR is better reproduced by RCA. The curvature effect attributed to the resonant waves also provides a better trend for the azimuth modulation amplitude. Figures 3c, 3d, 4c and 4d present the NRCS in both VV and HH polarizations separately for these two wind speeds which are the direct measurable quantities. As expected from our previous conclusions, RCA predicts a correct mean level for the NRCS in both HH and VV polarizations whereas LCA-1 and SSA-1 underestimate the NRCS in HH. As introduced with the curvature effect, the azimuthal modulation is naturally polarization sensitive. This fundamental aspect enables to predict a PR to be sensitive to geophysical parameters such as wind speed or wind direction relative to the radar's azimuth look direction. To be really complete with these data comparisons in C band, we present in Figures 3b and 4b the difference of NRCS $\sigma_0^{vv} - \sigma_0^{hh}$ in linear unit, DP hereafter, versus the wind direction relative to the radar's azimuth look direction for the two wind speeds considered here. Once again, RCA model is in overall good agreement with the data. DP quantity is interesting, as authors rapidly proposed to decompose the measured NRCS in a polarized and a scalar part [e.g., *Phillips*, 1988; *Chapron et al.*, 1997; *Quilfen et al.*, 1999]. Using DP quantity, we remove the scalar contribution to keep only the polarized part of the signal. In backscatter configuration, this part is taken into account through the first-order curvature correction term in LCA/RCA formalism.
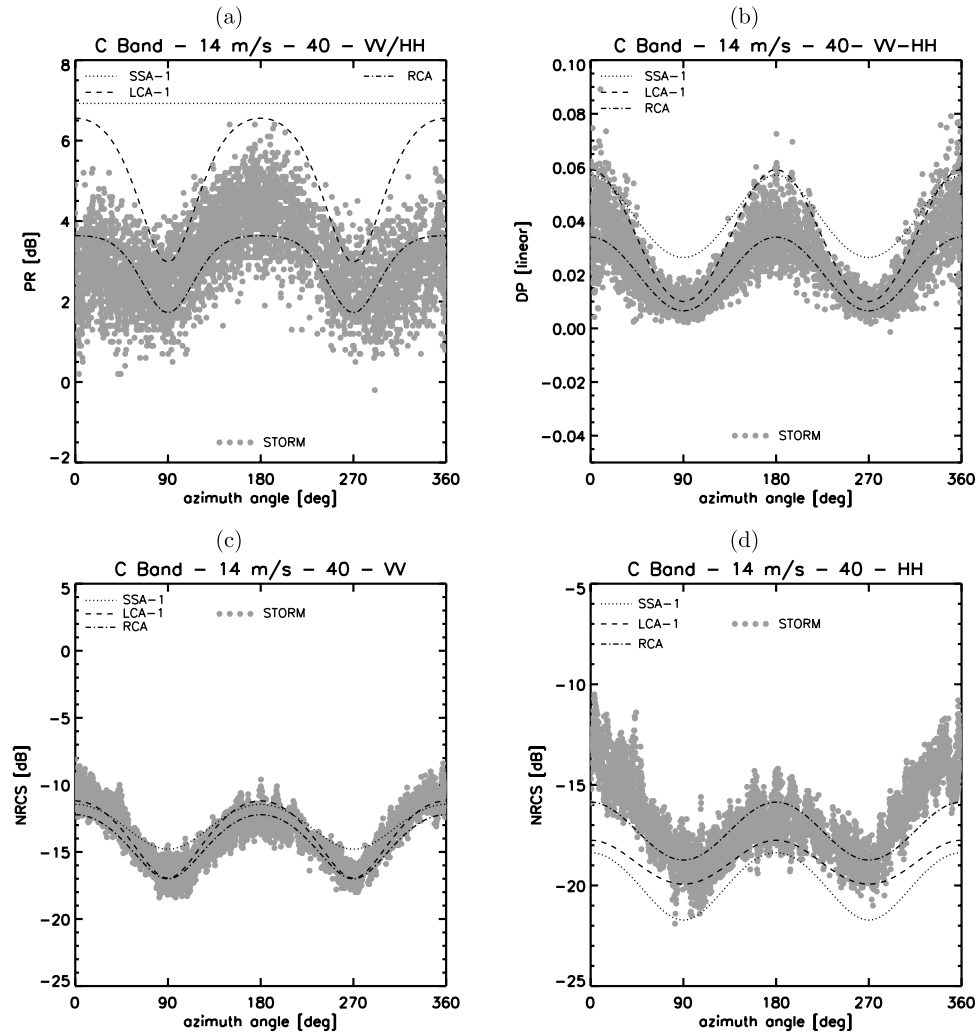
Figure 3. (a) Polarization ratio versus wind direction relative to the radar's azimuth look direction for a 11 m/s, a 40° incidence angle in C band. (b) Same but for the difference of NRCS. (c) Same but for the NRCS in VV polarization. (d) Same but for the NRCS in HH polarization. Data were acquired during the Valpareso experiment with STORM radar.

[19] To evaluate the ability of RCA to reproduce the data for different incident wavelengths, we also present a set of comparisons in X band. These data were collected during POLRAD'96 experiment. The wind speed considered here was provided by buoys, ships and/or model. The data set and the instrument were presented in detail by *Hauser et al.* [1997]. In Figure 5, as for STORM data, we present the PR (Figure 5a), DP (Figure 5b) and the NRCS (Figures 5c and 5d) in both copolarizations. In this case, from buoys and ship measurements, the wind speed is approximatively 8 m/s (we consider the mean of the four available measurements). As we already concluded for the C band, RCA/LCA formalism enables to reproduce an azimuth modulation for the PR, RCA predictions giving an excellent agreement with the data.

4.2. On the Skewness Effect on the NRCS

[20] In all the data presented here, we observe a difference between the NRCS levels observed upwind and downwind. This Upwind/Downwind Asymmetry (UDA hereafter) was already evidenced by many authors thanks

to radar data and is taken into account in the standard three-term Fourier model used for empirical formulations of the NRCS versus viewing angle with respect to wind direction. Measurements reveal that the NRCS level in upwind direction is greater than in downwind direction at high incidence angles (say > 30°) and lower at small incidence angles. In empirical models such as CMOD type models in C band or SASS in Ku band, the a_1 coefficient (see equation (1)) takes into account this small effect in the azimuth modulation. In physical models, a standard explanation for this asymmetry is done through the hydrodynamic modulation of Bragg waves. However, NSCAT Ku band data analysis combining the dual copolarization to remove the so-called scalar contribution [*Chapron et al.*, 1997] reveal that the contribution of the Bragg waves to the backscattered signal is larger downwind whereas the total UDA is directed upwind. This analysis proves that if the hydrodynamic modulation of Bragg waves exists, such an effect can be dominated by an other one. On the longer waves slopes, the lower amplitude Bragg waves are pre-

Figure 4. (a) Polarization ratio versus wind direction relative to the radar's azimuth look direction for a 14 m/s, a 40° incidence angle in C band. (b) Same but for the difference of NRCS. (c) Same but for the NRCS in VV polarization. (d) Same but for the NRCS in HH polarization. Data were acquired during the Valpareso experiment with STORM radar.

dominantly distributed windward. However, on the leeward side, the longer waves may be slightly steeper and rougher to decrease the polarized contribution. This explains the observed UDA in the DP signals reported by *Chapron et al.* [1997]. This implies that the opposite contribution to the UDA comes through the skewed form of the longer waves and the distribution of breaking waves which participate to the backscattering through the Kirchhoff mechanism. This idea to associate the UDA to breakers was applied by *Chapron et al.* [2002] and then by *Kudryavtsev et al.* [2003] in their NRCS model. To simply illustrate such an idea, we can consider the whole surface to be decomposed as $A = (1 - q) A + qA$, where q is the surface fraction covered by breaking waves [see *Kudryavtsev et al.*, 2003]. In this case, the total second-order moment becomes $\langle \eta^2 \rangle = (1 - q) \langle \eta_1^2 \rangle + q \langle \eta_2^2 \rangle$, where η_2 corresponds to the surface breakers, and η_1 to nonbreaking rough elements. Thus breaking waves contribute to second-order moments and thus to the spectrum or the correlation function. Hereafter,

our assumption is to consider that only breakers contribute to the third-order moment, such as $\langle \eta^3 \rangle = q \langle \eta_2^3 \rangle$.

[21] A skewness correction to the characteristic function enables to consider the modulated roughness distribution. Indeed, the characteristic function of a non-Gaussian random variable needs, to be completely defined, higher orders for the cumulants than only the second and the first. In the case of the sea surface, the statistical moments related to the second, third and fourth cumulants of the slopes were measured by Cox and Munk assuming a Gram Charlier's decomposition for the slope density function. Wave breaking events are relatively rare with extreme levels, and non-Gaussian statistics can be invoked. In the local frame of RCA model, the modified characteristic function up to the third order becomes

$$\langle e^{jQ_z(\bar{\eta}_2 - \bar{\eta}_1)} \rangle \approx e^{-Q_z^2(\bar{\rho}(0) - \bar{\rho}(\boldsymbol{r}))} e^{iQ_z^3 \tilde{S}_{\text{skew}}(\boldsymbol{r})}, \qquad (14)$$

where $\tilde{S}_{\text{skew}}$ is the skewness function. According to RCA formalism, any correcting order of the characteristic
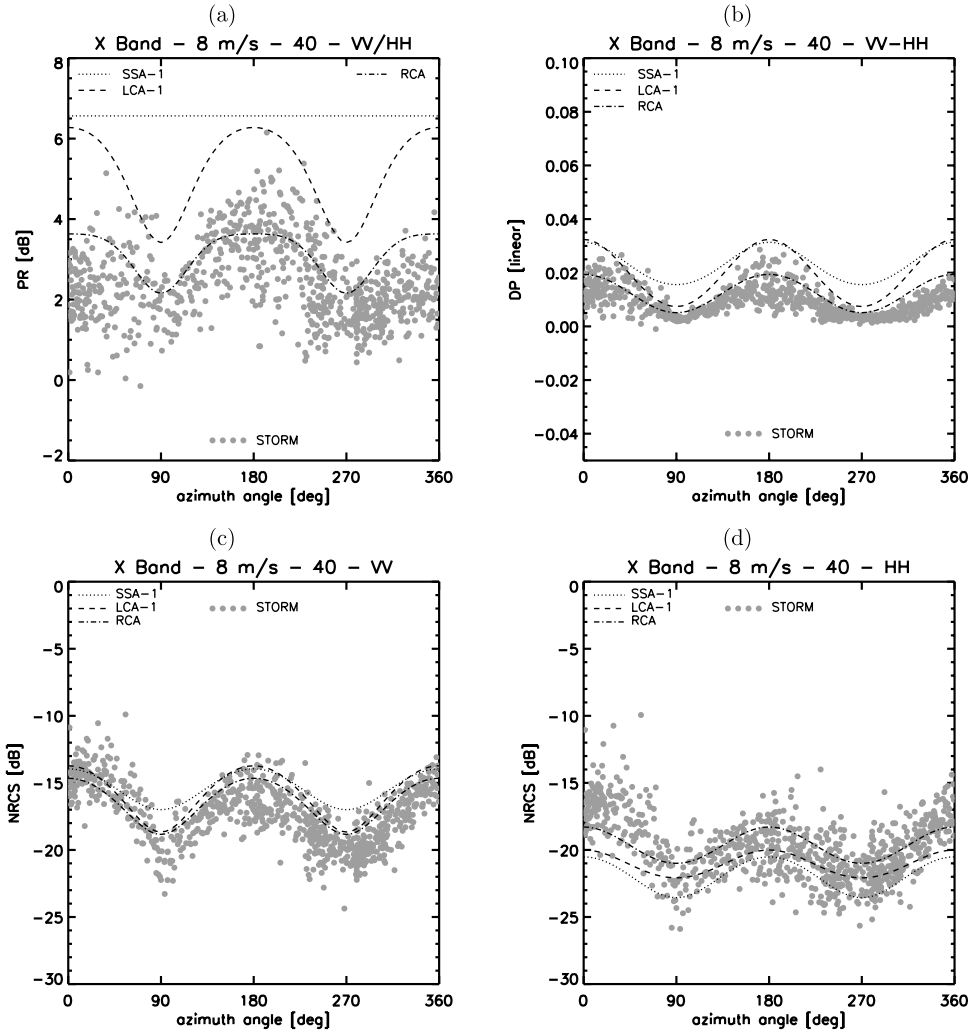
Figure 5. (a) Polarization ratio versus wind direction relative to the radar's azimuth look direction for a 8 m/s, a 40° incidence angle in X band. (b) Same but for the difference of NRCS. (c) Same but for the NRCS in VV polarization. (d) Same but for the NRCS in HH polarization. Data were acquired during the POLRAD experiment with RENE radar.

function can be polarization and frequency dependent. The NRCS when considering the skewness effect becomes

$$\sigma_0(\theta, \phi) = \left| \frac{\mathbb{K}(\boldsymbol{k}, \boldsymbol{k_0})}{Q_z} \right|^2 e^{-Q_z^2 \tilde{\rho}(0)} \int_{\boldsymbol{r}} \left[e^{Q_z^2 \tilde{\rho}(\boldsymbol{r}) + i Q_z^3 \tilde{S}_{\text{skew}}(\boldsymbol{r})} - 1 \right] e^{-i \boldsymbol{Q}_H \cdot \boldsymbol{r}} d\boldsymbol{r}. \tag{15}$$

[22] In this work we choose for the skewness function a generic formulation [*Elfouhaily*, 1997] adjusted on surface slope skewness when $\boldsymbol{r} \to 0$ [*Cox and Munk*, 1954]:

$$S_{\text{skew}}(\boldsymbol{r}) \underset{r \to 0}{=} -\frac{1}{6} x \sigma_{sx} \left(x^2 \sigma_{sx}^2 C_{03} + 3 y^2 \sigma_{sy}^2 C_{21} \right)$$

$$\approx -\frac{r^3}{6} \sigma_{sx}^3 C_{03} \cos(\phi), \tag{16}$$

$$S'_{\text{skew}}(0) = S''_{\text{skew}}(0) = S'''_{\text{skew}}(0) = 0 \tag{17}$$

where ϕ is the angle of the wind direction relative to the radar's azimuth look direction, σ_{sx}^2, σ_{sy}^2 the mean square

slopes in the up- and cross-wind direction, and C_{03}, C_{21} two empirical coefficients given by *Cox and Munk*'s [1954] measurements.

[23] In Figures 6a–6f, we present the UDA asymmetry of the NRCS in both copolarizations and of the PR as measured with STORM radar and compared with the prediction of RCA model when considering the skewness effect. To complete the data set, we also show the UDA given by two empirical models CMOD-IFREMER [*Quilfen et al.*, 1998] and CMOD-5 [*Hersbach et al.*, 2007]. Data indicate that the asymmetry is incidence, wind speed and polarization dependent. Results given by the RCA model give very good agreements with the data. In particular, RCA is able to predict realistic and different UDA for VV and HH polarizations. As a direct consequence, the predicted UDA for the PR is also in agreement with the data. In Ku band, we compared directly the a_1 coefficient in linear scale for a 10 and 15 m/s wind speed. We observe on Figure 7 that the trend with incidence angle is rather well reproduced by the model thanks to the third-order correction in the characteristic function.
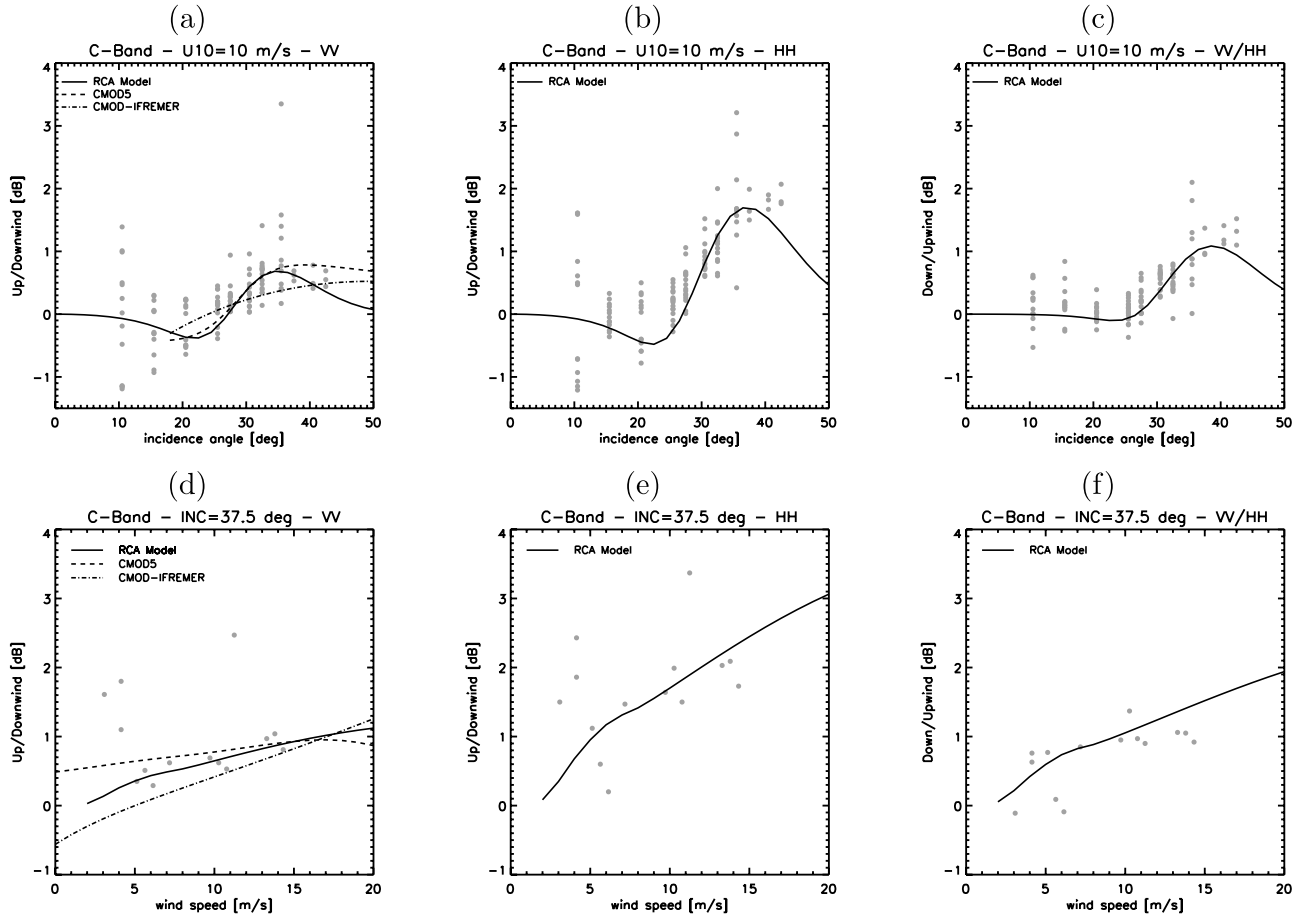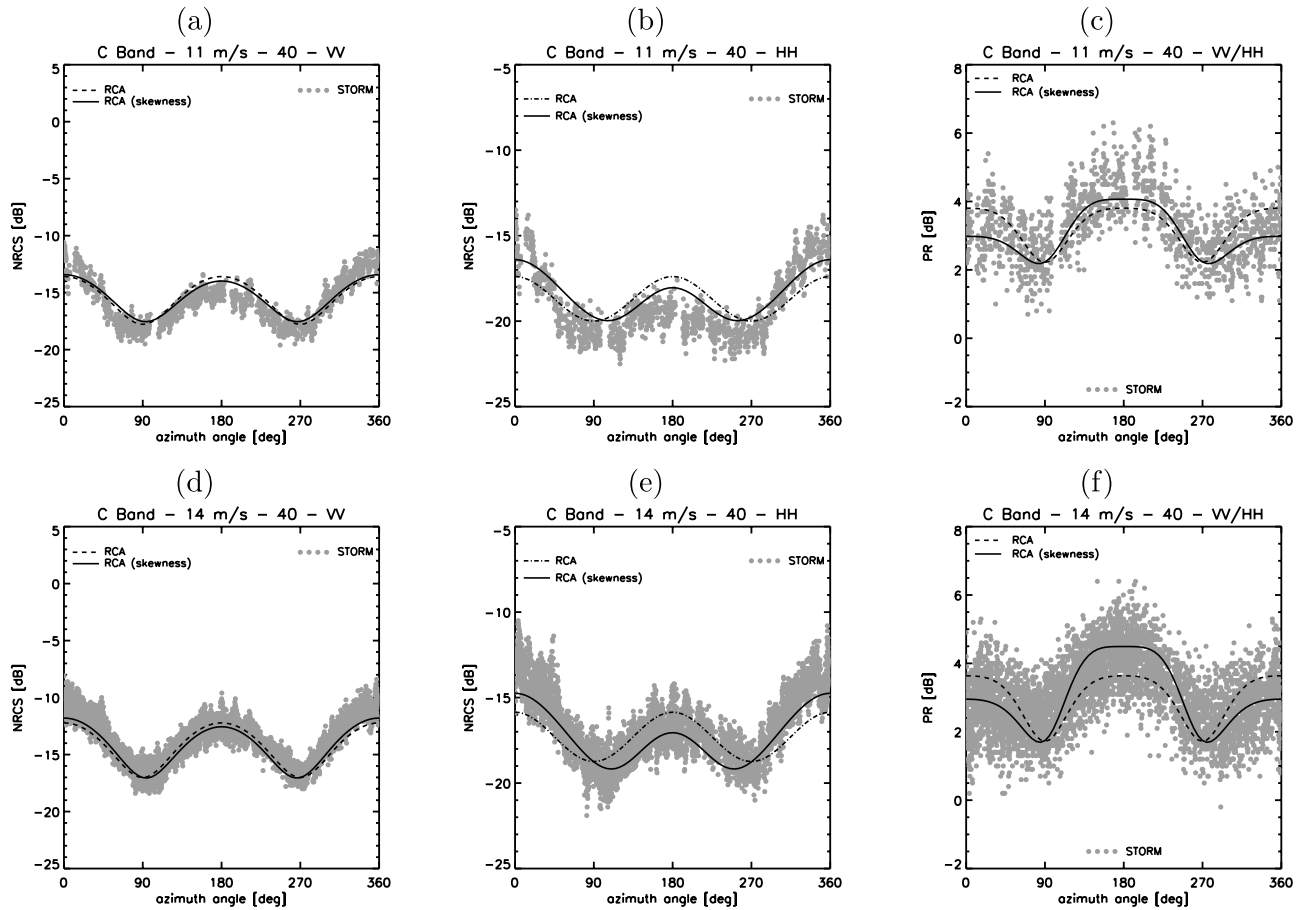
Figure 6. UDA versus incidence angle in (a) VV and (b) HH polarizations for a 10 m/s. (c) Downwind to upwind asymmetry of the PR versus incidence angle for a 10 m/s. UDA versus incidence angle for (d) VV and (e) HH polarizations for a 37.5° incidence angle. (f) Downwind to upwind asymmetry of the PR versus incidence angle for a 37.5° incidence angle. Data were acquired during the VALPARESO experiment with STORM radar.
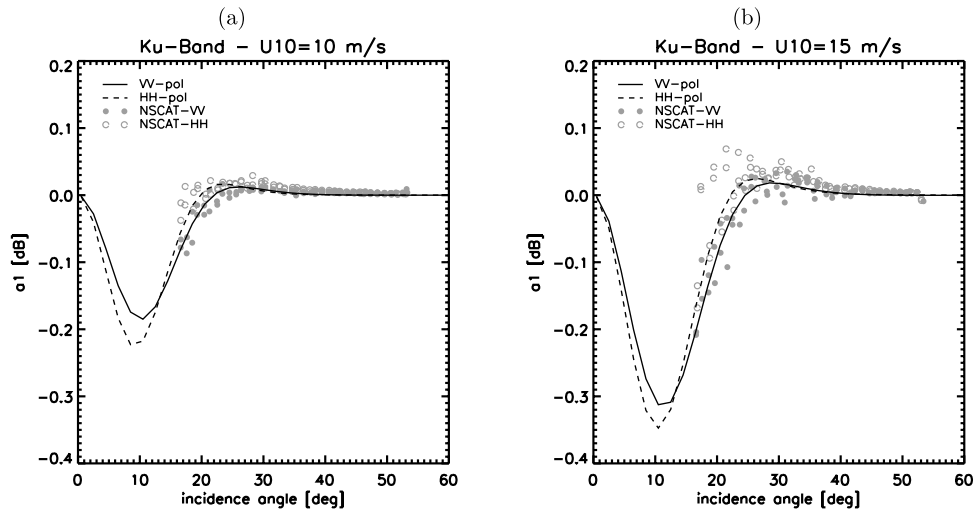
Figure 7. The a_1^{vv} and a_1^{hh} coefficients as a function of the incidence angle in Ku band for two given 10-m-high wind speeds: (a) 10 m/s and (b) 15 m/s. Data are from NSCAT.

Figure 8. NRCS versus wind direction relative to the radar's azimuth look direction for a 11 m/s 10-m-high wind speed, a 40° incidence angle in C band in (a) VV and (b) HH polarizations. (c) Same for the PR. NRCS versus wind direction relative to the radar's azimuth look direction for a 14 m/s 10-m-high wind speed, a 40° incidence angle in C band in (d) VV and (e) HH polarizations. (f) Same for the PR. Data were acquired during the VALPARESO experiment with STORM radar.

[24] Taking into account the skewness according to equation (15) also modifies the azimuth modulation. The results from RCA are reported with and without skewness effect in Figure 8 for comparisons with data. We observe that, compared to the case of a Gaussian assumption, accounting the third-order correction gives more realistic trends for the NRCS as a function of relative azimuth angles with a significant difference between up- and down-wind configurations. As observed and predicted, this effect is greater in HH than in VV polarization.

5. Conclusion

[25] We consider the sea surface curvature influence on the radar backscatter measurements. Two asymptotic solutions, LCA-1 and RCA, were applied to the case of scattering from a two-dimensional sea surface and compared with other existing models. Comparisons with data showed that RCA results are in overall good agreement with the data whereas LCA results are very close to the TSM predictions. This difference between the two models comes from the fact that the RCA limits the curvature effect to the resonant Bragg waves.

[26] The formalism of LCA/RCA has the advantage to take into account the depolarization effect of the sea surface through a dynamical first-order term in the scattering matrix expansion (equation (7)). Indeed, its impact depends on both the configuration of the instrument (incidence, frequency and polarization) and the sea surface curvature properties. This is a key element for an improved understanding of the electromagnetic and oceanic waves interactions. In the framework of RCA, the first-order term in the scattering matrix expansion enables to reproduce the NRCS in both copolarization versus incidence angle in the microwave domain. Good agreements for each polarization allows the model to reproduce the mean level and the azimuthal modulation of PR. This leads to conclude that the curvature correction impacts on the polarization is certainly necessary. Considering satisfying semiempirical results given by *Kudryavtsev et al.* [2003] and *Kudryavtsev et al.* [2005], a parallel between these approaches is to recognize the scalar zeroth order of RCA with the breaking waves and longer waves contribution invoked by Kudryavtsev and coauthors, while the curvature correction term and the Bragg contribution could be associated to the same scattering process of the short resonant waves. RCA does not need a

dividing parameter to separate short and large scales of the sea surface. Moreover, as the enhanced roughness zones contribution may be hard to precisely parameterize, it could be convenient to use a model such as RCA which consider both contributions from regular and nonregular surface implicitly through the statistical correlation function. In a future work, an explicit comparison of these two models approaches will be done. However, as an important issue, it can be stated that PR modulations shall follow the roughness strength and distribution.

[27] Finally, we discussed the implication of the non-Gaussian statistics on the NRCS for the sea surface description. Interestingly, it appears from RCA formalism that the characteristic function of the scattered field is polarization, incidence and frequency dependent. Moreover, RCA is in agreement with *Chapron et al.*'s [1997] conclusion about the UDA of the Bragg waves and breaking waves at large incidence angle. Taking into account a third-order correction term in the characteristic function as a signature of breaking waves, it appears that extraction of the third moment in the backscattered signal would be interesting to improve our understanding of the impact of breaking events on the NRCS.

[28] A model such as RCA can further be used to improve our understanding about the backscatter signal modulations. At large incidence angles the NRCS in HH is lower than for the VV polarization, to indicate that the sensor is more sensitive to the small waves in VV polarization. For HH polarization, it is the contrary which means that the sensor is more sensitive to the longer and steeper waves in this configuration. At large incidence angles, such a sensitivity to the faster traveling longer and steeper waves than the slower resonant Bragg waves will induce a larger Doppler shift. Future use of the proposed model will be to refine our current understanding and use of the combined measured Doppler shifts and backscatter signals [*Mouche et al.*, 2007b].

Appendix A: NRCS Expression of Existing in the Case of Gaussian Statistics

[29] For convenience, we recall here the expression of the NRCS for SPM-1, TSM, SSA-1 and KA models as they are used through the paper. The derivation is done in case of Gaussian statistics. We consider the same coordinates system and definitions than those used to express the RCA solution in section 3 but also in the review on approximated wave scattering theories from random rough surfaces proposed by *Elfouhaily and Guérin* [2004]. $\boldsymbol{K} = (\boldsymbol{k}, q_k)$ and $\boldsymbol{K}_0 = (\boldsymbol{k}_0, -q_0)$ respectively denotes the wave numbers of the scattered and incident waves. $\mathbb{B}(\boldsymbol{k}, \boldsymbol{k}_0)$ and $\mathbb{K}(\boldsymbol{k}, \boldsymbol{k}_0)$ are the so-called kernels of Bragg and Kirchhoff Approximations. Their expression is given by *Elfouhaily et al.* [2003b]. $\boldsymbol{Q}_H = \boldsymbol{k} - \boldsymbol{k}_0$ and $Q_z = q_k + q_0$.

A1. Small Perturbation Method at First Order

$$\sigma_0^{BR} = 16\pi k_0^4 |\mathbb{G}(\boldsymbol{k}, \boldsymbol{k}_0)|^2 S(\boldsymbol{Q}_H), \qquad (A1)$$

[30] where $S(\boldsymbol{Q}_H)$ is the wave number folded spectrum of the surface elevations. $\mathbb{G}(\boldsymbol{k}, \boldsymbol{k}_0)$ is the scattering coefficient [see, e.g., *Plant*, 1990].

A2. Two-Scale Model

$$\sigma_0^{TSM} = \int_{-\infty}^{\infty} d(\tan\Psi) \int_{-\infty}^{\infty} d(\tan\delta)\sigma_0^{BR}(\theta_i)P(\tan\Psi, \tan\delta), \quad (A2)$$

[31] where $P(\tan\Psi, \tan\delta)$ is the joint probability density of slopes for the long waves, θ_i the local angle, and $\sigma_{0_{BR}}$ the NRCS given by the SPM-1 due to the small roughness elements modulated by the longer waves. In our calculation this probability density is assumed Gaussian. The calculation of $\sigma_{0_{BR}}$ is done considering the angles corrections given by *Elfouhaily et al.* [1999] instead of initial Valenzuela's results [*Valenzuela*, 1978],

$$\theta_i = -\cos^{-1}\left[\cos(\theta + \Psi)\cos(\tan^{-1}\delta\cos\Psi)\right]$$

with $S_x = \tan\Psi$ and $S_y = \tan\delta$, the slopes of longer waves in and perpendicular to the incident plane.

A3. Small Slope Approximation at First Order

$$\sigma_0^{SSA-1} = \left|\frac{\mathbb{B}(\boldsymbol{k}, \boldsymbol{k}_0)}{Q_z}\right|^2 e^{-Q_z^2\rho(0)}\int_r \left[e^{Q_z^2\rho(r)} - 1\right]e^{-i\boldsymbol{Q}_H\cdot\boldsymbol{r}}d\boldsymbol{r}. \quad (A3)$$

A4. Kirchhoff Approximation

$$\sigma_0^{KIR} = \left|\frac{\mathbb{K}(\boldsymbol{k}, \boldsymbol{k}_0)}{Q_z}\right|^2 e^{-Q_z^2\rho(0)}\int_r \left[e^{Q_z^2\rho(r)} - 1\right]e^{-i\boldsymbol{Q}_H\cdot\boldsymbol{r}}d\boldsymbol{r}. \quad (A4)$$

References

Berman, D., and D. Dacol (1990), Manifestly reciprocal scattering amplitudes for rough surfaces interface scattering, *J. Acoust. Soc. Am.*, *87*, 2024–2032.

Chapron, B., V. Kerbaol, and D. Vandemark (1997), A note on relationships between sea-surface roughness and microwave polarimetric backscatter measurements: Results form POLRAD'96, in *Proceedings of the International Workshop POLRAD'96, ESA Publ. WPP-135*, pp. 55–64, Eur. Space Agency, Noordwijk, Netherlands.

Chapron, B., D. Vandemark, and T. Elfouhaily (2002), On skewness of the sea slope probability distribution, in *Gas Transfer at Water Surfaces, Geophys. Monogr. Ser.*, vol. 127, edited by M. Donelan, et al., pp. 59–64, AGU, Washington, D. C.

Chapron, B., F. Collard, and V. Kerbaol (2004), Satellite synthetic aperture radar sea surface Doppler measurements, in *Proceedings of the 2nd Workshop on Coastal and Marine Applications of SAR, ESA Rep. SP-565*, pp. 133–140, Eur. Space Agency, Noordwijk, Netherlands.

Chapron, B., F. Collard, and F. Ardhuin (2005), Direct measurements of ocean surface velocity from space: Interpretation and validation, *J. Geophys. Res.*, *110*, C07008, doi:10.1029/2004JC002809.

Cox, C., and W. Munk (1954), Measurements of the roughness of the sea surface from photographs of the Sun's glitter, *J. Opt. Soc.*, *44*, 838–850.

Elfouhaily, T. (1997), A consistent wind and wave model and its application to microwave remote sensing of the ocean surface, Ph.D. diss., Denis Diderot Univ., Paris.

Elfouhaily, T., and C.-A. Guérin (2004), A critical survey of approximate scattering wave theories from random rough surfaces, *Waves Random Media*, *14*, R1–R40.

Elfouhaily, T., B. Chapron, K. Katsaros, and D. Vandemark (1997), A unified directionnal wave spectrum for long and short wind-driven waves, *J. Geophys. Res.*, *102*, 15,781–15,796.

Elfouhaily, T., D. Thompson, D. Vandemark, and B. Chapron (1999), A new bistatic model for electromagnetic scattering from perfectly conducting random surfaces, *Waves Random Media*, *9*, 281–294.

Elfouhaily, T., S. Guignard, R. Awdallah, and D. Thompson (2003a), Local and non-local curvature approximation: A new asymptottic theory for wave scattering, *Waves Random Media*, *13*, 321–337.

Elfouhaily, T., M. Joelson, S. Guignard, and D. Thompson (2003b), Analytical comparison between the surface current integral equation and the second-order small slope approximation, *Waves Random Media*, *13*, 165–176.

Hauser, D., P. Dubois, and G.Caudal (1997), Polarimetric wind-scatterometer measurements during POLRAD'96, in *Proceedings of the International Workshop POLRAD'96*, *ESA Publ. WPP-135*, pp. 55–64, Eur. Space Agency, Noordwijk, Netherlands.

Hauser, D., T. Podvin, M. Dechambre, R. Valentin, G. Caudal, and J.-F. Daloze (2003), STORM: A new polarimetric real aperture radar for Earth observations, paper presented at the ESA POLinsar International Workshop, Eur. Space Agency, Noordwijk, Netherlands.

Hersbach, H., A. Stoffelen, and S. de Haan (2007), An improved C-band scatterometer ocean geophysical model function: CMOD5, *J. Geophys. Res.*, *112*, C03006, doi:10.1029/2006JC003743.

Kelly, K., S. Dickinson, M. McPhaden, and G. Johnson (2001), Ocean currents evident in satellite wind data, *Geophys. Res. Lett.*, *28*, 2469–2472.

Kudryavtsev, V., D. Hauser, G. Caudal, and B. Chapron (2003), A semi-empirical model of the normalized radar cross-section of the sea surface: 1. Background model, *J. Geophys. Res.*, *108*(C3), 8055, doi:10.1029/2001JC001004.

Kudryavtsev, V., D. Akimov, J. Johannessen, and B. Chapron (2005), On radar imaging of current features: 1. Model and comparison with observations, *J. Geophys. Res.*, *110*, C07016, doi:10.1029/2004JC002505.

Monaldo, F., and V. Kerbaol (2003), The sar measurement of ocean surface winds: An overview, in *Proceedings of the 2nd Workshop on Coastal and Marine Applications of SAR*, *ESA Rep. SP-565*, pp. 15–32, Eur. Space Agency, Noordwijk, Netherlands.

Mouche, A., D. Hauser, J.-F. Daloze, and C. Guérin (2005), Dual-polarization measurements at C-band over the ocean: Results from ariborne radar observations and comparison with ENVISAT ASAR data, *IEEE Trans. Geosci. Remote Sens.*, *43*, 753–769.

Mouche, A. A., D. Hauser, and V. Kudryavtsev (2006), Radar scattering of the ocean surface and sea-roughness properties: A combined analysis from dual-polarizations airborne radar observations and models in C band, *J. Geophys. Res.*, *111*, C09004, doi:10.1029/2005JC003166.

Mouche, A. A., B. Chapron, and N. Reul (2007a), A simplified asymptotic theory for ocean surface electromagnetic wave scattering, *Waves Random Complex Media*, *17*(3), 321–341.

Mouche, A. A., B. Chapron, N. Reul, and F. Collard (2007b), Predicted Doppler shifts induced by ocean surface displacements using asymptotic electromagnetic wave scattering theories, *Waves Random Complex Media*, in press.

Park, K.-A., P. Cornillon, and D. Codiga (2006), Modification of surface winds near ocean fronts: Effects of Gulf Stream rings on scatterometer (QuikSCAT, NSCAT) wind observations, *J. Geophys. Res.*, *111*, C03021, doi:10.1029/2005JC003016.

Phillips, O. (1988), Radar returns from the sea surface—Bragg scattering and breaking waves, *J. Phys. Oceanogr.*, *18*, 1063–1074.

Plant, W. (1986), A two-scale model of short wind-generated waves and scatterometry, *J. Geophys. Res.*, *91*, 10,735–10,749.

Plant, W. (1990), Bragg scattering of electromagnetic waves from the air/sea interface, in *Surface Waves and Fluxes: Current Theory and Remote Sensing*, edited by G. Geernaert and W. Plant, pp. 41–108, Springer, New York.

Plant, W. J. (2002), A stochastic, multiscale model of microwave backscatter from the ocean, *J. Geophys. Res.*, *107*(C9), 3120, doi:10.1029/2001JC000909.

Quilfen, Y., B. Chapron, T. Elfouhaily, K. Katsaros, and J. Tournadre (1998), Observation of tropical cyclones by high resolution scatterometry, *J. Geophys. Res.*, *103*, 7767–7786.

Quilfen, Y., B. Chapron, A. Bentamy, J. Gourrion, T. Elfouhaily, and D. Vandermark (1999), Global ERS-1 and 2 NSCAT observations: Upwind/crosswind and upwind/downwind measurements, *J. Geophys. Res.*, *104*, 11,459–11,469.

Quilfen, Y., B. Chapron, and D. Vandemark (2001), The ERS scatterometer wind measurement accuracy: Evidence of seasonal and regional biaises, *J. Atmos. Oceanic Technol.*, *18*, 1684–1697.

Shaw, W., and A. Dougan (1998), Green's function refinement as an approach to radar backscatter: General theory and application to LGA scattering from the ocean, *IEEE Trans. Antenna Propag.*, *46*, 57–66.

Valenzuela, G. (1978), Theories for the interactions of electromagnetic and oceanic waves—A review, *Boundary Layer Meteorol.*, *13*, 61–85.

Voronovich, A. (1994), Small-slope approximation for electromagnetic wave scattering at a rough interface of two dielectric half-spaces, *Waves Random Media*, *4*, 337–367.

Voronovich, A., and V. Zavarotny (2001), Theoretical model for scattering of radar signals in KU- and C-bands from a rough sea surface with breaking waves, *Waves Random Media*, *11*, 247–269.

––––––––––––––––––

B. Chapron, A. A. Mouche, Y. Quilfen, and N. Reul, Laboratoire d'Océanographie Spatiale, Ifremer, Z.I. Pointe du Diable, B.P.70, F-29280 Plouzané, France. (bchapron@ifremer.fr; alexis.mouche@ifremer.fr; yquilfen@ifremer.fr; nreul@ifremer.fr)

D. Hauser, Centre d'Etude des Environnements Terrestre et Planétaires, IPSL, CNRS/UVSQ, 1-12, Avenue de l'Europe, F-78140 Vélizy, France. (daniele.hauser@cetp.ipsl.fr)